Electronic Supplementary Material (ESI) for Journal of Materials Chemistry A.

High-Performance Cupric Oxide Photocatalyst with Palladium Light Trapping Nanostructures and Hole Transporting Layer for Photoelectrochemical Hydrogen Evolution

Saeid Masudy-Panah,[1,2,#] Reza Katal,[3,#] Negar Dasineh Khiavi,[4] Ehsan Shekarian,[5] Jiangyong Hu[3] and Gong Xiao [1,2,*]

[1]Electrical and Computer Engineering, National University of Singapore, Singapore 119260

[2]Low Energy Electronic Systems (LEES), Singapore-MIT Alliance for Research and Technology (SMART) Centre, Singapore

[5]Department of Civil & Environmental Engineering, National University of Singapore, Singapore 119260

[4]Faculty of Biosciences & Medical Engineering, Universiti Teknologi Malaysia

[5]SEPPURE Laboratory, 79 Ayer Rajah Crescent, Singapore 139955

[#]These authors contributed equally.

[*]Corresponding authors email: elegong@nus.edu.sg

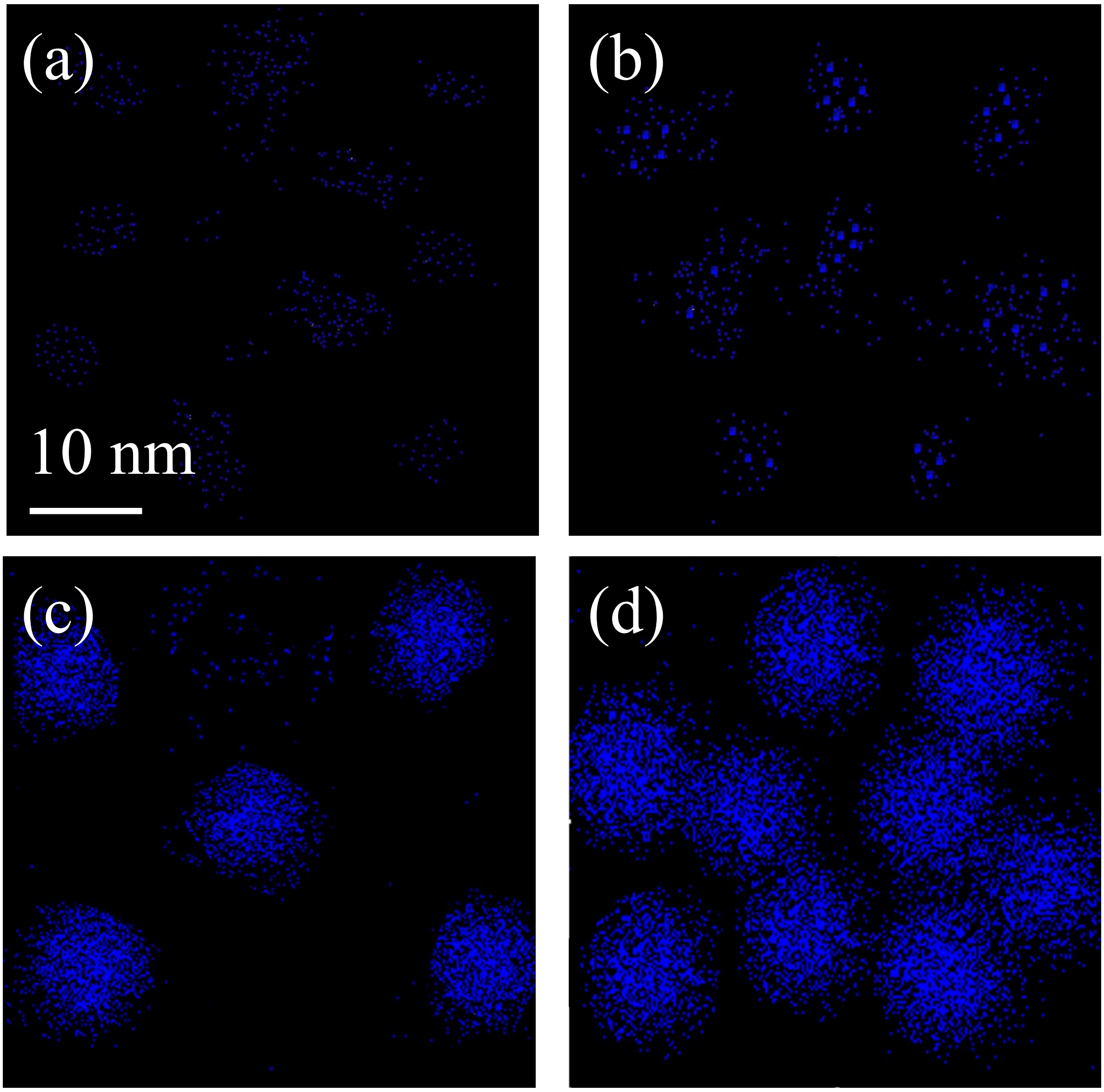

Fig. S1 EDX elemental mapping of Pd nanostructures of CuO:Pd photocathodes deposited at CuO sputtering power of 300 W and Pd sputtering power of (a) 5, (b) 15, (c) 30, (d), and 50 W.

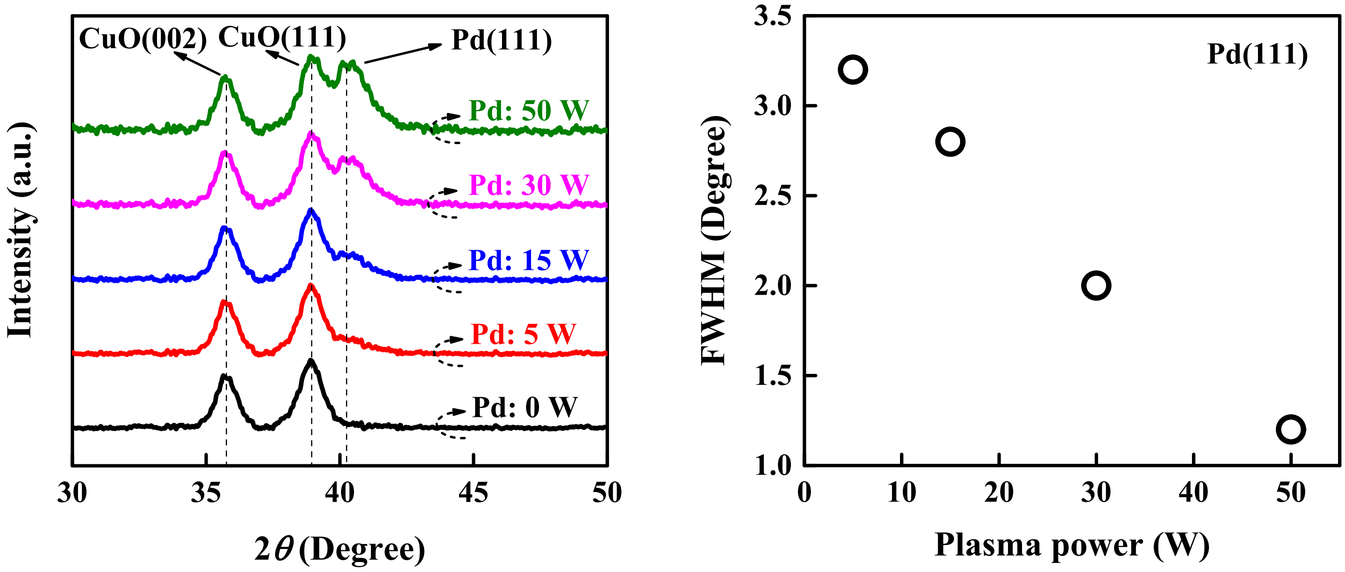

(a)

(b)

Fig. S2 (a) XRD spectra of the CuO:Pd thin film and (b) full width half maximum (FWHM) of the main Pd XRD peak deposited at Pd sputtering power of 0-50 W. The intensity of Pd(111) peak becomes more pronounced and its corresponding FWHM significantly reduces by increasing the Pd sputtering.

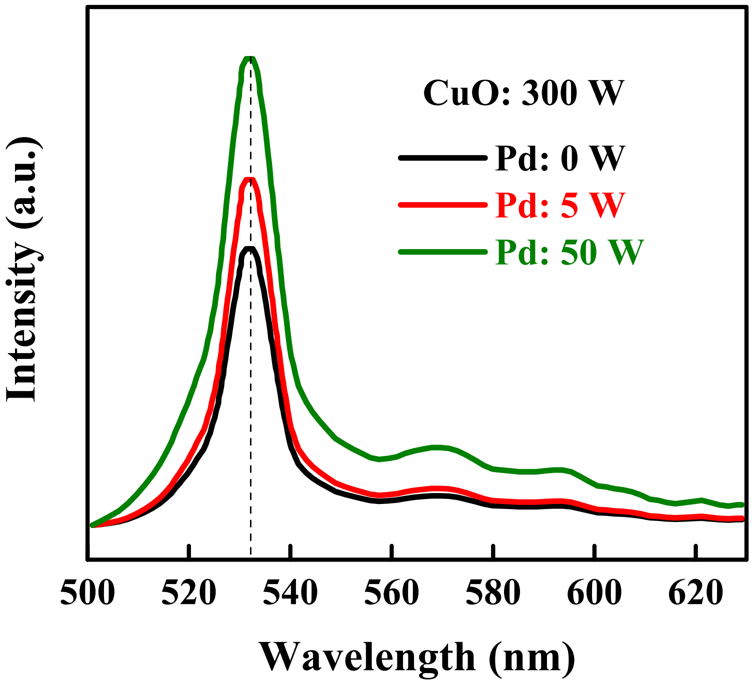

Fig. S3 Photoluminescence of CuO:Pd prepared at CuO sputtering power of 300 W and Pd sputtering power of 0, 5, and 50 W. Intensity of photoluminescence CuO:Pd samples significantly enhances by increasing the Pd sputtering.

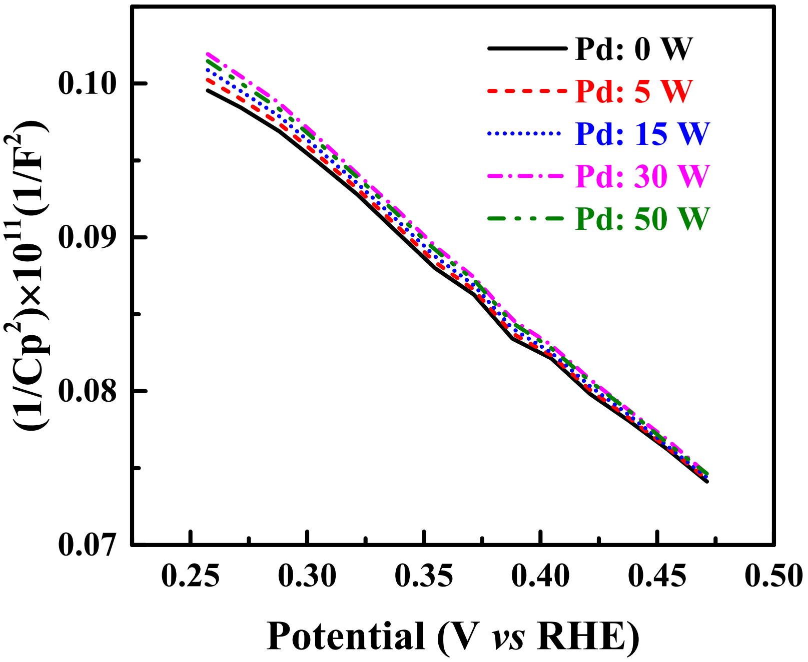

Fig. S4 Mott–Schottky plot of CuO:Pd photocathodes fabricated with Pd sputtering power of 0-50 W. The x-intercept and the slope of the extrapolated linear part of the M-S curve is used to estimate the values of N_A and V_{FB}.

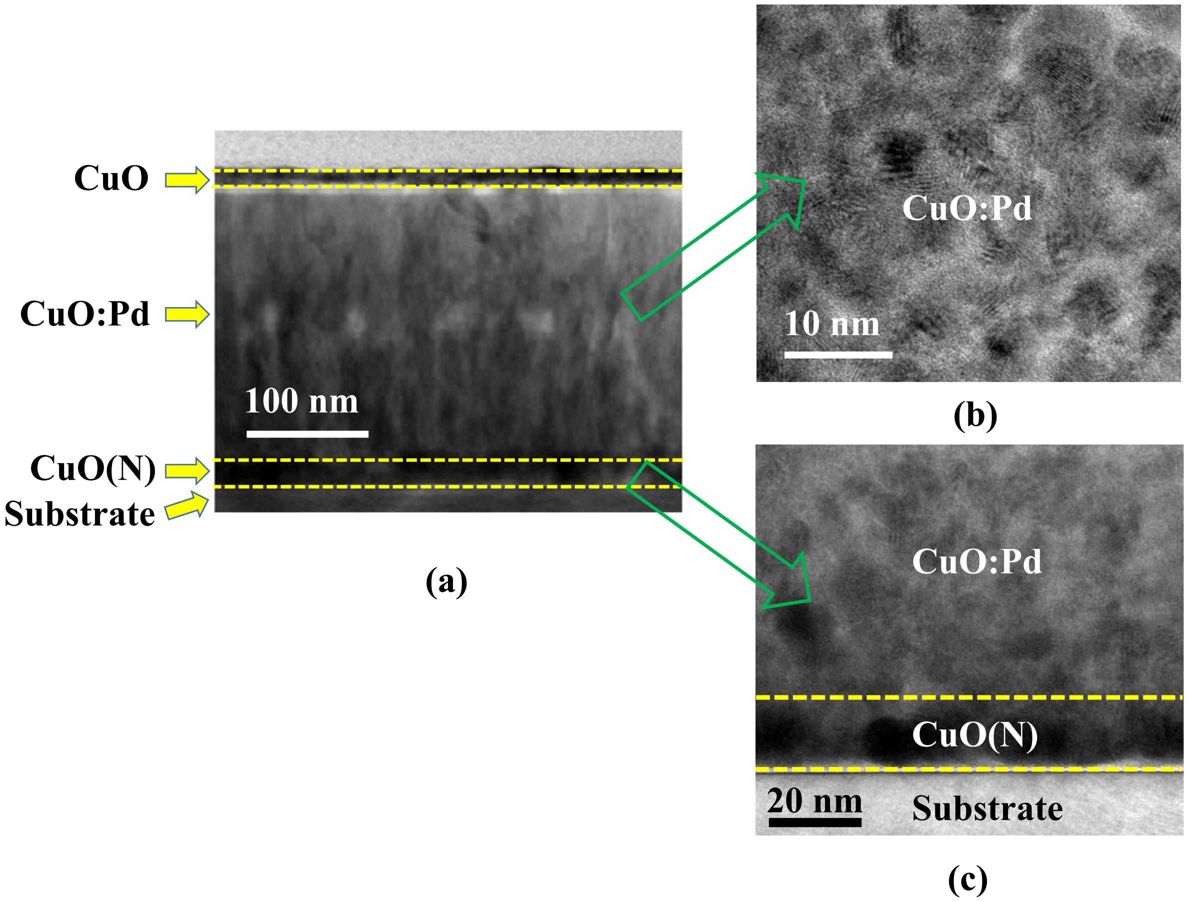

(a)

(b)

(c)

Fig. S5. (a) Cross-sectional, (b) high resolution, and (c) high resolution cross-sectional TEM images of CuO(N)-CuO:Pd-CuO thin films deposited at CuO sputtering power of 300 W, Pd sputtering power of 30 W, and N gas flow rate of 10 sccm. The thickness of the CuO capping layer and CuO(N) transporting layer are around 15 and 20 nm, respectively.

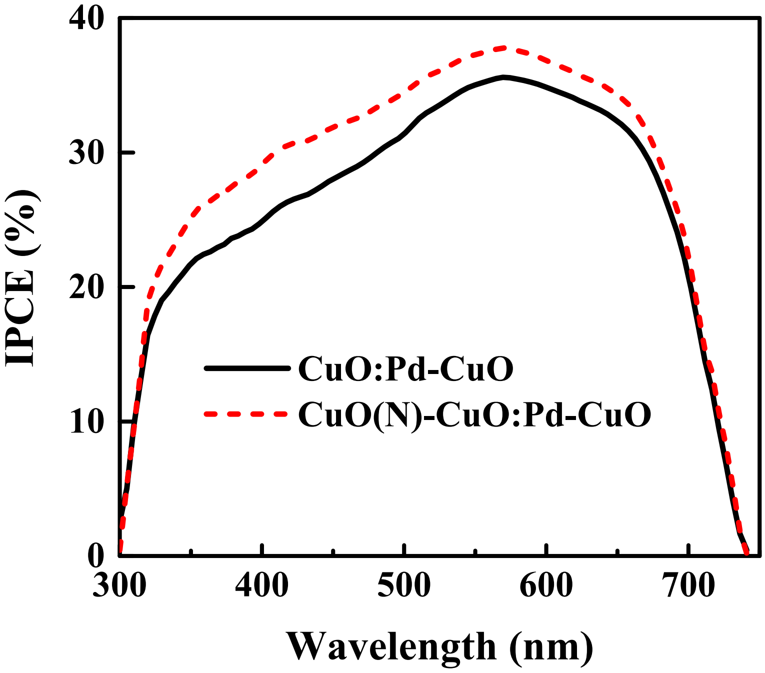

Fig. S6. IPCE of CuO:Pd-CuO and CuO(N)-CuO:Pd-CuO photocathodes fabricated with Pd and CuO sputtering power of 30 and 300 W, respectively. The IPCE of CuO(N)-CuO:Pd-CuO photocathode is higher than the CuO:Pd-CuO photocathode in the 320-690 nm wavelength range. This indicates the effectiveness of incorporating the CuO(N) hole transporting layer in photo-generated charge carriers separation.

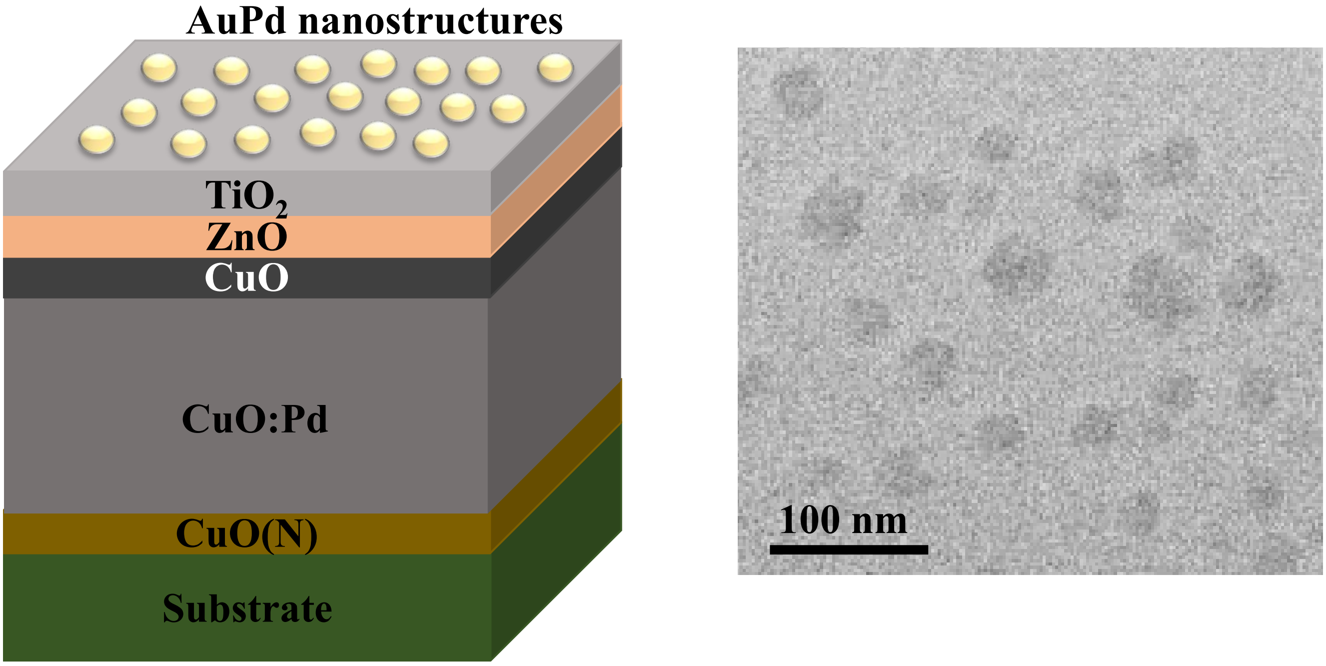

(a) (b)

Fig. S7. (a) Schematic diagram and (b) top view TEM of CuO(N)-CuO:Pd-CuO-ZnO-TiO_2 photocathode decorated with AuPd nanoparticles. Diameter of AuPd nanoparticles is around 30 nm.

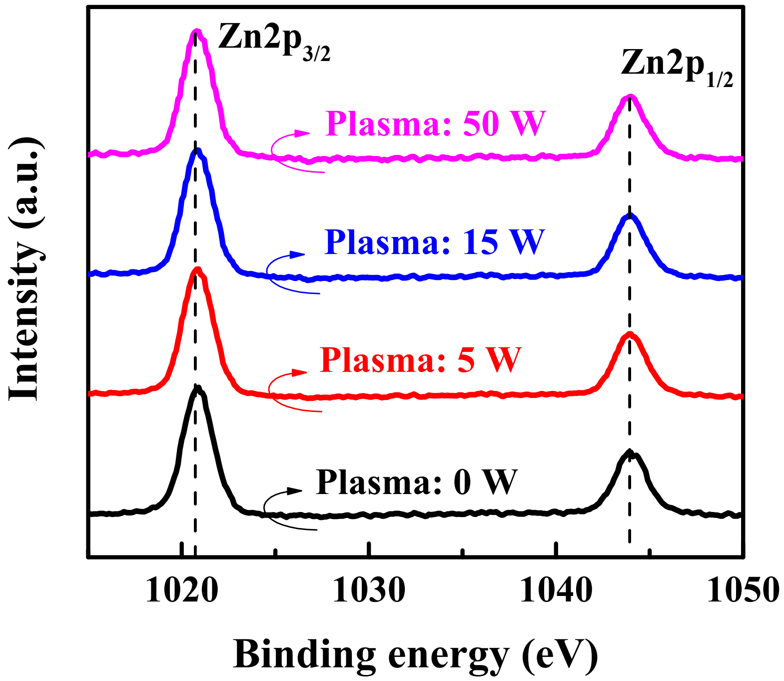

(a)

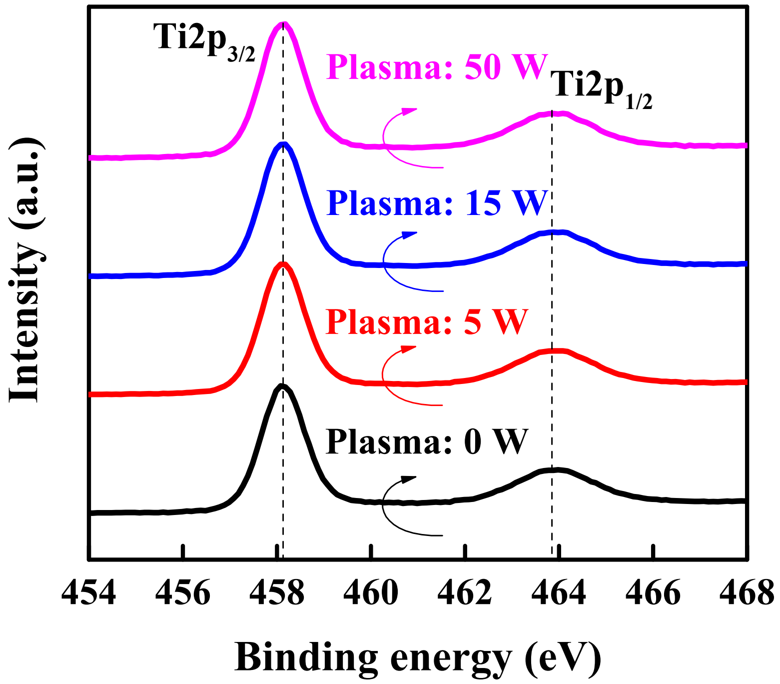

(b)

Fig. S8 High-resolution (a) Zn 2p and (b) Ti 2p core-level XPS spectra of the ZnO buffer layer and TiO_2 protective layers, respectively. Increasing the *in-situ* plasma power does not affect the chemical composition of deposited ZnO and TiO_2 thin films.

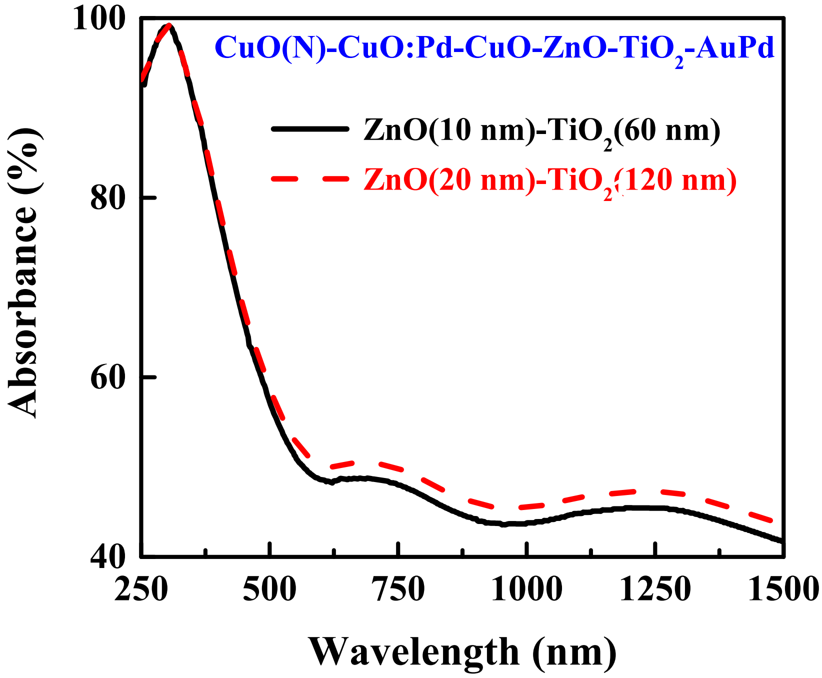
CuO(N)-CuO:Pd-CuO-ZnO-TiO$_2$-AuPd
ZnO(10 nm)-TiO$_2$(60 nm)
ZnO(20 nm)-TiO$_2$(120 nm)
Absorbance (%)
100
80
60
40
250
500
750
1000
1250
1500
Wavelength (nm)

(a)

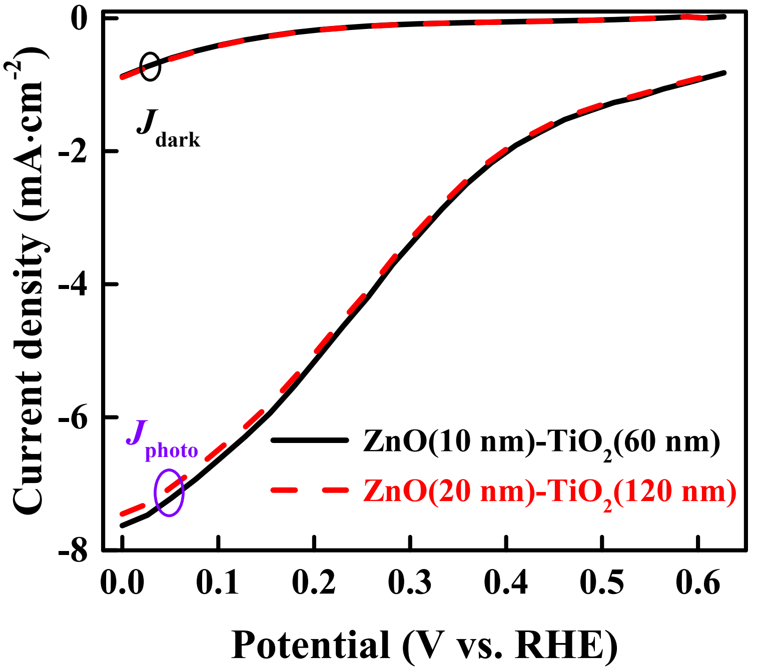
J_{dark}
J_{photo}
ZnO(10 nm)-TiO$_2$(60 nm)
ZnO(20 nm)-TiO$_2$(120 nm)
Current density (mA·cm^{-2})
0
-2
-4
-6
-8
0.0
0.1
0.2
0.3
0.4
0.5
0.6
Potential (V vs. RHE)

(b)

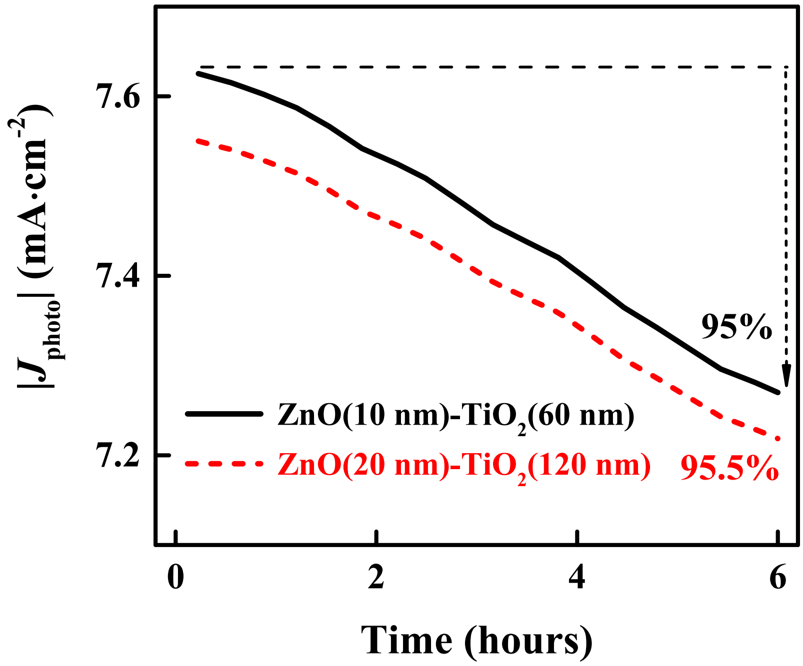

(c)

Fig. S9. (a) Optical absorbance, (b) current density, and (c) photocorrosion stability of CuO(N)-CuO:Pd-CuO-ZnO-TiO$_2$ with different thickness of ZnO and TiO$_2$.

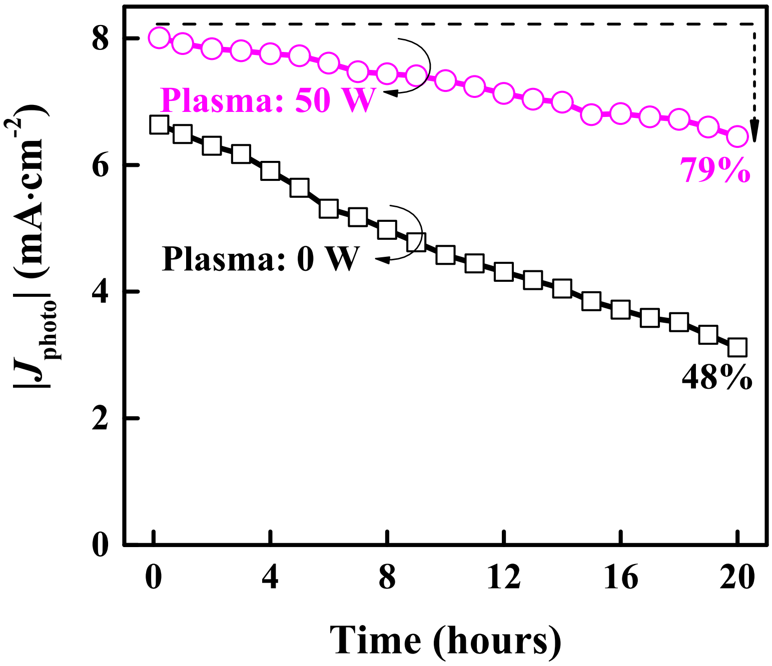

Fig. S10. Photocorrosion stability of CuO(N)-CuO:Pd-CuO-ZnO-TiO_2-AuP photocathodes prepared at different *in-situ* plasma treatment power for prolonged time of 20 hours.

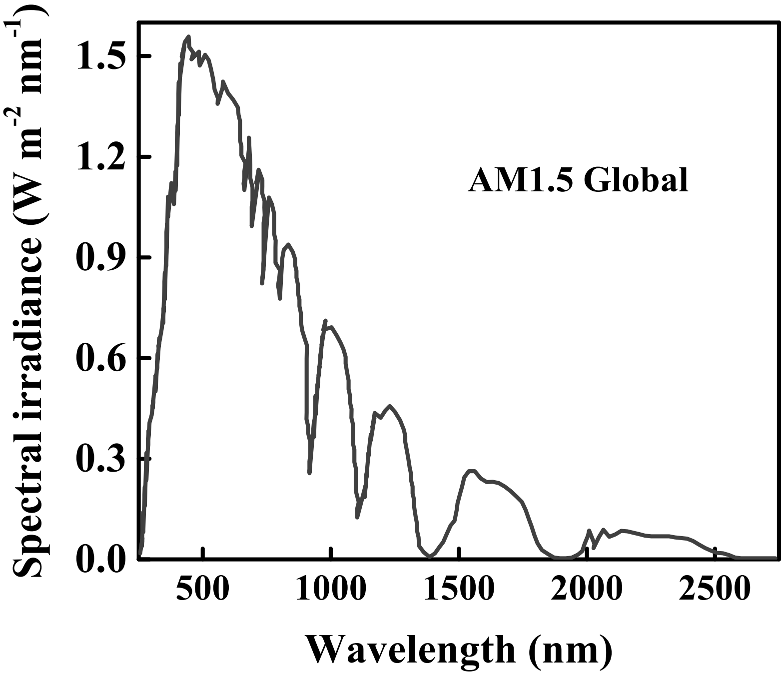

(a)

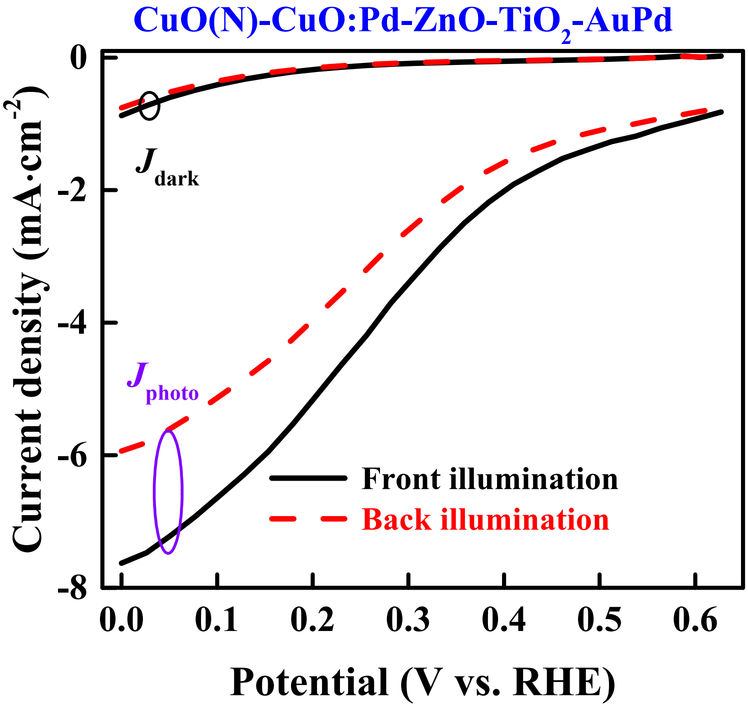

(b)

Fig. S11. (a) spectral irradiance and (b) current density under back and front illumination. Photocurrent density under the back illumination is significantly lower than the photocurrent density under the front illumination.